ARTICLE

Single Particle Quantum Dot Imaging Achieves Ultrasensitive Detection Capabilities for Western Immunoblot Analysis

Benjamin Scholl,[†] Hong Yan Liu,[†] Brian R. Long,[†] Owen J. T. McCarty,[†] Thomas O'Hare,[‡,§] Brian J. Druker,[‡,§] and Tania Q. Vu[†,*]

[†]Department of Biomedical Engineering, [‡]Division of Hematology & Medical Oncology, Oregon Health and Science University, Portland, Oregon 97239, and [§]Howard Hughes Medical Institute

ABSTRACT Substantially improved detection methods are needed to detect fractionated protein samples present at trace concentrations in complex, heterogeneous tissue and biofluid samples. Here we describe a modification of traditional Western immunoblotting using a technique to count quantum-dot-tagged proteins on optically transparent PVDF membranes. Counts of quantum-dot-tagged proteins on immunoblots achieved optimal detection sensitivity of 0.2 pg and a sample size of 100 cells. This translates to a 10^3-fold improvement in detection sensitivity and a 10^2-fold reduction in required cell sample, compared to traditional Westerns processed using the same membrane immunoblots. Quantum dot fluorescent blinking analysis showed that detection of single QD-tagged proteins is possible and that detected points of fluorescence consist of one or a few (<9) QDs. The application of single nanoparticle detection capabilities to Western blotting technologies may provide a new solution to a broad range of applications currently limited by insufficient detection sensitivity and/or sample availability.

KEYWORDS: Western blot · quantum dot · electrophoresis · single molecule · proteomics · immunoblot

Western immunoblotting is a low-cost and simple cornerstone technology that is used in virtually all biomedical laboratories for detecting cellular proteins.[1,2] An indispensable feature of Western immunoblotting is its capability to fractionate and determine the size of specific proteins, thus making it a favored technique for routine protein analysis of complex biomixtures. Despite widespread use, Western immunoblotting faces significant limitations in detection sensitivity, making it difficult or impossible to use in situations requiring detection of trace proteins (less than 1 ng) or scarce biosamples (less than 10^5–10^6 cells).[3] Detecting Western immunoblot signals at the level of single fluorescent tags would achieve the ultimate sensitivity limit in Western immunoblotting technology and allow even broader application of this invaluable technique.

Recently, we and others have used intensely bright, multicolor emitting quantum dot (QD) nanoparticles as substitute fluorescent tags for detection of proteins following electrophoretic separation and immobilization onto membranes. These studies showed that QD tags allow simultaneous viewing of different colors, serve as a platform for gel pull-downs of cellular proteins, and importantly, increase protein detection sensitivity—all with significantly decreased experimental time and effort.[4–6] In these recent QD-based Western blot studies, the QD fluorescent signal emanating from the blot was detected as a bulk, integrated fluorescent signal. Using bulk QD fluorescence, Bakalova *et al.* showed a substantial improvement in protein blot detection sensitivity when bright QD tags were used in place of traditional HRP chemiluminescent tags.[5] However, the detection of bulk QD fluorescence was not sensitive enough to capture all available QD signals. An incremental improvement in detection sensitivity (by 2–5-fold) was attained by attaching multiple QDs to each antibody probe in an effort to increase QD intensity.[5]

The ultimate limit in sensitive detection of Western blot signals can be reached by detecting probes with single particle resolution. Because the bright fluorescence emission of QDs allows them to be imaged on glass as single particles, we hypothesized that we could further extend the sensitivity of Western immunoblotting technology by quantifying proteins tagged at the level of individual QDs. Here, we report a method to image discrete QD-tagged proteins that

*Address correspondence to tvu@bme.ogi.edu.

Received for review January 13, 2009 and accepted May 07, 2009.

Published online May 19, 2009.
10.1021/nn9000353 CCC: $40.75

are immobilized on membranes by converting opaque PVDF membranes into optically transparent siloxane-treated PVDF membranes. This enables analysis of Western blot signals at the resolution of discrete fluorescent points of QD-tagged protein and is a contrast to traditional analysis of bulk blot bands. We show that the capability to count discrete QD-tagged proteins allows significant increase in sensitivity and reduction in the amount of cell sample. Application of this single nanoparticle detection capability to Western blotting technologies may provide a new solution to a broad range of applications currently limited by insufficient detection sensitivity and/or sample availability.

RESULTS

Our method of detecting and counting discrete QDs in transparent PVDF membranes, called single point quantum dot (SPQD) Western blotting, is outlined in Figure 1A. A key step of this method is converting the PVDF membranes from an opaque to an optically transparent state, thus allowing high-quality detection and quantification of QD-tagged proteins. Single QDs are easily detected on glass slides using a fluorescent microscope,[7−9] but stable fluorescence detection of single QDs on PVDF membranes is a substantial problem: PVDF membranes are opaque (Figure 1B) and existing methods using alcohol-based solvents (*e.g.*, methanol) for producing semi-transparent membranes are not only poor for detecting single QDs (Supporting Information Figure 1S) but are also not compatible with preserving membrane-adsorbed protein for subsequent immunoblotting steps.

To image proteins tagged with QDs on PVDF membranes, we follow a simple and cheap method using commercially available materials. We immerse dry, opaque PVDF membranes in polydimethylsiloxane (PDMS) mixtures such as PDMS curing agent (see Methods). The PDMS curing agent penetrates dry PVDF membranes and creates an optically transparent PDMS−PVDF membrane mixture that allows single QDs to be detected using a simple fluorescent microscope (Figure 1B, left-hand column). Note that QDs cannot be detected on opaque PVDF membranes (Figure 1B, right-hand column). Using PDMS−PVDF membranes, it is possible to detect single points of QD fluorescence that are stable and persist for >10 min under continuous excitation. In contrast, QD fluorescence rapidly quenches (<1 min) in buffers, such as those used in traditional Western immunoblotting protocols. PDMS−PVDF membranes can be stored in a cold room (4 °C) and can be reimaged with single QD detection quality for long periods after blot preparation (3−6 weeks).

The mechanism of the PDMS-induced PVDF transparency is a physical interaction between PDMS and PVDF, based on several lines of evidence. First, this mechanism is reversible—that is, a transparent PDMS−PVDF membrane can be reverted to an opaque state by physically wiping and washing the PDMS agent to remove it from the transparent PDMS−PVDF. Second, while we have not found published work reporting the transparent transforming properties of PDMS with PVDF, it is known in the polymer field that PDMS will physically interlace with other polymers to produce hybrid materials known as semi-interpenetrating polymer networks, defined by virtue of their physical (noncovalent interactions).[10,11] Finally, the effect of PDMS−PVDF transparency is not specifically rendered by one particular type of PDMS, which would more likely be characteristic of a specific covalent chemical interaction. We routinely use Sylgard 184 silicone curing agent (Methods), which contains a combination of dimethyl, methylhydrogen siloxane and dimethylsiloxane dimethylvinyl-terminated and tetramethyl tetravinyl cyclotetrasiloxane; however, other polydimethylsiloxane mixtures such as methyl-terminated polydimethylsiloxane, or the combination of siloxanes present in the base portion of Sylgard 184 elastomer, are also effective in converting PVDF to transparent PDMS−PVDF membranes. Physical penetration of the PDMS agent into the disordered and fibrous PVDF membrane may provide a better match in the index of refraction at the PDMS−PVDF interface compared to the index of refraction at the air−PVDF interface, thereby decreasing scattering and increasing transparency of the membrane.

The new capability to detect single points of QD fluorescence makes possible the measurement of QD fluorescent bands at lower concentrations that would otherwise remain invisible. Figure 1C shows that while it is possible to detect macroscopic bands of fractionated QD bioconjugates (biotin-QD655s, and streptavidin-QD655s) at relatively high concentrations (2.5 nM: lanes 2 and 4) using a UV transillumination table, in contrast, QD bioconjugates are not visible at low concentrations (25 pM: lanes 1 and 3). After the opaque PVDF membrane was converted to a transparent PDMS−PVDF membrane, single points of QD fluorescence could be resolved at both high and low QD concentrations (bottom panel, Figure 1C).

On the basis of several observations, the discrete points of QD fluorescence we detected were an accurate representation of blot bands typically measured by averaged integration (*e.g.*, densitometry). First, lanes loaded with lower quantities of QD bioconjugates (lanes 1 and 3) contained fewer points of discrete QD fluorescence than lanes loaded with higher amounts of QD bioconjugates (lanes 1 and 3). Second, automated scanning along the length of the lanes containing low amounts of QDs (Figure 2C, lanes 1 and 3) showed that the QD distribution corresponded to the distribution visible by eye of high density QD bands (Figure 2C, right panel). Automated counting for relatively high numbers of QDs (lanes 2 and 4) was difficult due to the dense grouping of individual QDs and due to the con-

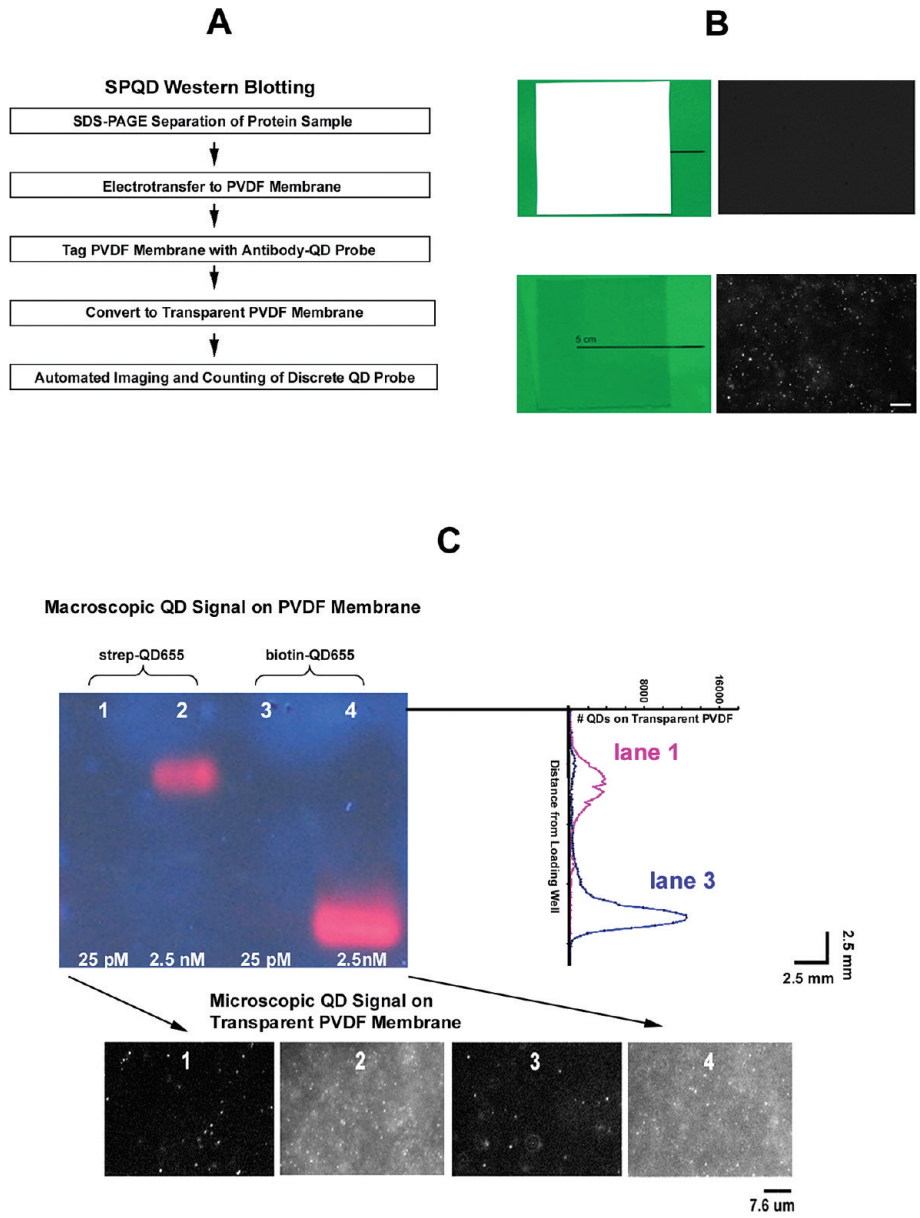

Figure 1. Counts of single point of QD fluorescence allow accurate quantification of fluorescent blot bands at low concentration. (A) Schematic of single point quantum dot (SPQD) Western Immunoblotting. (B) Detection of discrete QD fluorescence is possible on PDMS-treated PVDF membranes but not using opaque PVDF membranes. *Left-hand side:* opaque and transparent nature of the PVDF and PDMS−PVDF membrane, respectively, shown by simultaneously scanned images of these membranes placed atop a printed scale bar on a green background. *Right-hand side:* transparent PDMS−PVDF membranes enable quality, discrete QD detection that is not possible with opaque PVDF membranes. Microscopic images taken with a CCD camera mounted on a fluorescence microscope under same conditions; scale: 7.2 um. (C) *Top row:* After gel separation and electrotransfer of two QD bioconjugate species, macroscopic UV illumination shows that relatively high concentrations of QDs are visible, but low concentrations of QDs are not (streptavidin-QD655s: lanes 1 and 2: 2.5 nM and 25 pM each at 3 μL; biotin-QD655s: lanes 2 and 4: 2.5 nM and 25 pM each at 3 μL). *Bottom row:* After PDMS treatment of PVDF membrane blots (above), microscope images taken of membrane at the location of bright macroscopic QD bands (above) show the presence of discrete QD fluorescence. Almost all points of QD fluorescence showed blinking at all loading concentrations, an indicator that each fluorescent count is composed of individual or small numbers of QDs (Supporting Information movie). Image acquisition and processing are the same for all images. *Right-hand panel:* Plots of lanes containing low QD signal (lanes 1 and 3) are graphed as number of QD counts/micrograph *vs* distance from loading well, illustrating that QD counts accurately reflect that of macroscopic blots seen by the eye at higher QD concentrations (lanes 2 and 4). Graph represents 180 micrographs taken in a band area of 3.2 mm × 1.9 mm.

tribution of diffuse fluorescence emitted by out-of-focus QDs (during electrotransfer, QDs enter PVDF membranes over a depths of ~1 um). Finally, virtually all discrete points of QD fluorescence exhibited fluctuations, indicating that counts were composed of individual or small numbers of QDs (Supporting Information Movie 2S). A standard used to identify single QDs from a group is QD fluorescent "on−off" blinking: evidence that QD fluorescence intensity returns to a dark "off" state that is indistinguishable from the back-

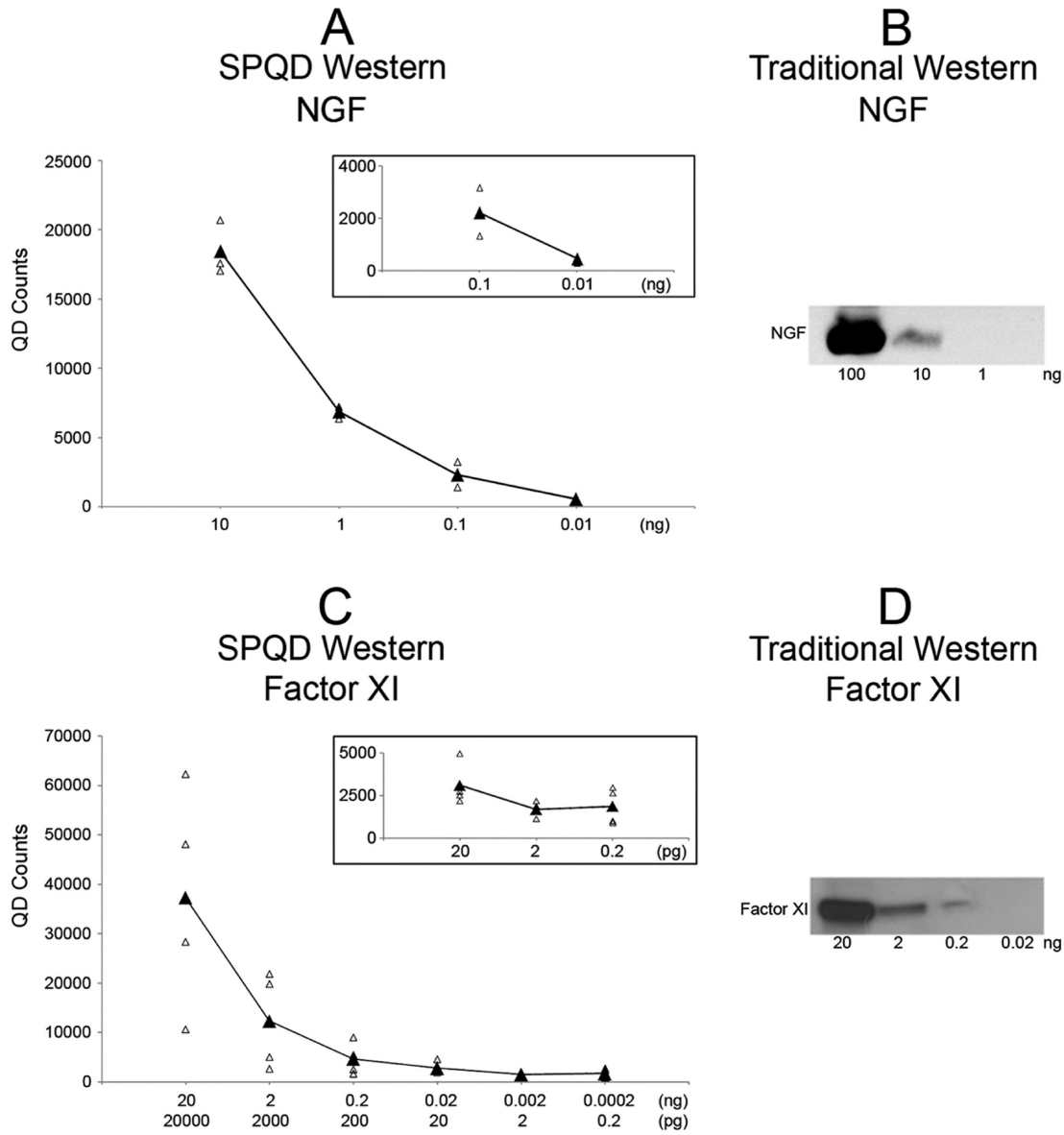

Figure 2. Single point quantum dot Western immunoblotting achieves enhanced protein detection sensitivity. (A) Purified protein detection performed using SPQD for nerve growth factor (NGF) shows a detection sensitivity of 0.01 ng. Plot inset shows QD counts for the lowest protein amounts (0.1 and 0.01 ng). SPQD Western QD counts were acquired from a total of $n = 3$ independent experiments in a band area of 3.3 mm × 0.50 mm ($n = 1$) and 3.3 mm × 1.9 mm ($n = 2$): (△) independent trials; (▲) mean. (B) In comparison, traditional Western blots performed using the same NGF-fractionated membranes as in A show a detection threshold of 10 ng. (C) Detection threshold of SPQD blots for purified protein standards of Factor XI show a detection sensitivity of 0.2 pg. SPQD Western QD counts were acquired from $n = 4$ independent experiments in a band area of 1 mm × 3 mm. Plot inset shows QD counts for the lowest protein amounts (20−0.2 pg): (△) independent trials; (▲) mean. (D) Traditional Western blots performed using the same Factor XI membranes in C show a detection threshold of 0.2 ng. All measurements were normalized by subtracting QD counts from parallel blank control lanes containing buffer in each experiment.

ground fluorescence.[8,12,13] Discrete QD counts exhibited square wave shaped on−off blinking in time-varying intensity profiles, demonstrating that we detect single QDs on these transparent PDMS−PVDF membranes (see Supplementary Figure 3S and Figure 5 for further extensive analysis).

Detection of two different samples of purified, fractionated proteins showed that SPQD Westerns provide a substantial increase in protein detection sensitivity. SPQD Westerns were performed using a polyclonal anti-NGF antibody to detect purified nerve growth factor (NGF), a hormone protein implicated with a number of pathophysiological conditions.[14,15] SPQD Westerns yielded a detection threshold of 0.01 ng (Figure 2A), compared to detection of 10 ng by traditional Westerns that were processed using the same membrane blots (Figure 2B). This was a 10^3-fold improvement in the sensitivity of SPQD Westerns in comparison to traditional Westerns. SPQD Westerns were also performed using a monoclonal anti-Factor XI antibody that binds to a single epitope site on Factor XI, a protein present at low concentrations in plasma.[16] SPQD Westerns of Fac-

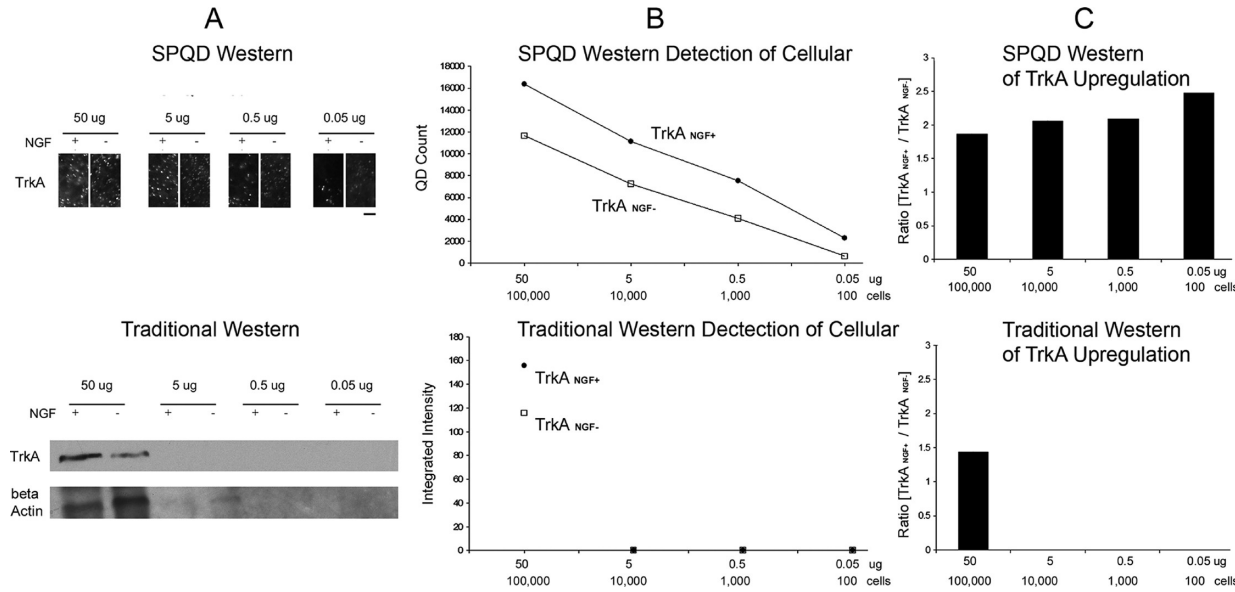

Figure 3. Single point quantum dot Western immunoblotting provides a significant reduction of the amounts of required cell sample. (A) Cellular protein detection performed for TrkA receptor protein in PC12 cells using SPQD and traditional Western blots. TrkA levels measured for steady-state (NGF−) and stimulated (NGF+) levels. SPQD Western signal's detection threshold is 0.05 ng (100 cells). A limited region of the membrane is shown to demonstrate the discrete nature of QD counts of TrkA over all range tested (scale: 6.4 μm). Traditional Western blot's signal is 50 μg of cell sample (100 000 cells). Similar cell amounts are required for abundant actin protein (loaded into parallel lanes of same membrane). (B) TrkA levels plotted as a function of amount of cell sample. TrkA signal quantified as arbitrary integrated intensity (traditional Westerns) and QD counts (SPQD blotting) SPQD blotting results computed from band area of 3.3 mm × 1.9 mm. All values normalized by subtraction from parallel blank control lanes loaded with buffer. (C) Graph of TrkA upregulation ($TrkA_{NGF+}/TrkA_{NGF-}$). TrkA upregulation is detectable by SPQD Westerns over the entire range of 0.05−50 μg (10^2−10^5 cells) compared to the Western blot threshold of 50 μg (10^2 cells).

tor XI yielded a detection threshold of 0.2 pg (Figure 2C) compared to detection of 0.2 ng by traditional Westerns (Figure 2D). Again, this was a 10^3-fold sensitivity increase in comparing the SPQD Western and traditional Western techniques. SPQD counts for each protein concentration of both Factor XI and NGF were performed over multiple independent trials and yielded values above the background. In particular, for low sample amounts, the number of QD-tagged proteins could be distinguished from the background of nonspecifically bound QDs, as seen by values that are consistently located above the *x*-axis (Figure 2). Our optimal sensitivity for the detection of pure protein was 0.2 pg. This translates to a 10^3-fold increase in sensitivity over traditional Westerns performed on the same blots and a 5×10^3-fold increase in sensitivity over the 1 ng sensitivity limit reported by bulk fluorescence measurements using QD-based Western immunoblots.[5]

We then applied the SPQD Western blotting technique to cellular samples and found that specific proteins of interest could be detected in as few as 100 cells. SPQD and traditional Westerns were performed to detect the TrkA tyrosine kinase receptor protein, as well as TrkA upregulation induced by exposing PC12 cells with NGF, a TrkA cognate ligand. In SPQD Westerns, TrkA receptor protein could be detected in samples of 10^2−10^3 cells, translating to an amount of 0.05−0.5 μg of total protein (Figure 3A). Traditional Western immunoblots were performed on samples run in adjacent lanes of the same membrane and required a minimum of 10^5 cells or 50 μg of protein (Figure 3B). Cells treated with NGF have an increase in TrkA production, and by using SPQD blotting, we were able to detect a subtle increase in protein production (×1.5−2) for samples as few as 100 cells (Figure 3C). Traditional Westerns using these same cell lysate samples produced a detectable signal for a sample of 10^5 cells. Traditional Westerns were also used to detect actin, an abundant protein in these same cell samples. An amount of 10^5 cells was still required to produce a detectable signal (Figure 3A). These results demonstrate that SPQD Western immunoblot technology can provide a detectable signal in cell samples of as few as 100 cells. This is a 10^3−10^4-fold improvement over typical ranges of 10^5−10^6 cells used in traditional Westerns and is a 10^2-fold over QD-based Western immunoblots.[5]

To further verify this level of sensitivity in cellular samples, we performed SPQD and traditional Western blots using a two-antibody method in which one antibody detects total CrkL protein and the other detects the phosphorylated form of CrkL protein. CrkL is a direct substrate of the oncogenic tyrosine kinase, BCR-ABL, the causative molecular lesion in chronic myeloid leukemia (CML). Detection of CrkL phosphorylation is the preferred pharmacodynamic assay for CML clinical trials involving new BCR-ABL inhibitors.[17,18] Figure 4A shows that the detection threshold of SPQD Westerns for each antibody−protein pair was 100 cells. This SPQD threshold is 10^3 times greater than traditional Westerns performed with the total-CrkL antibody (Fig-

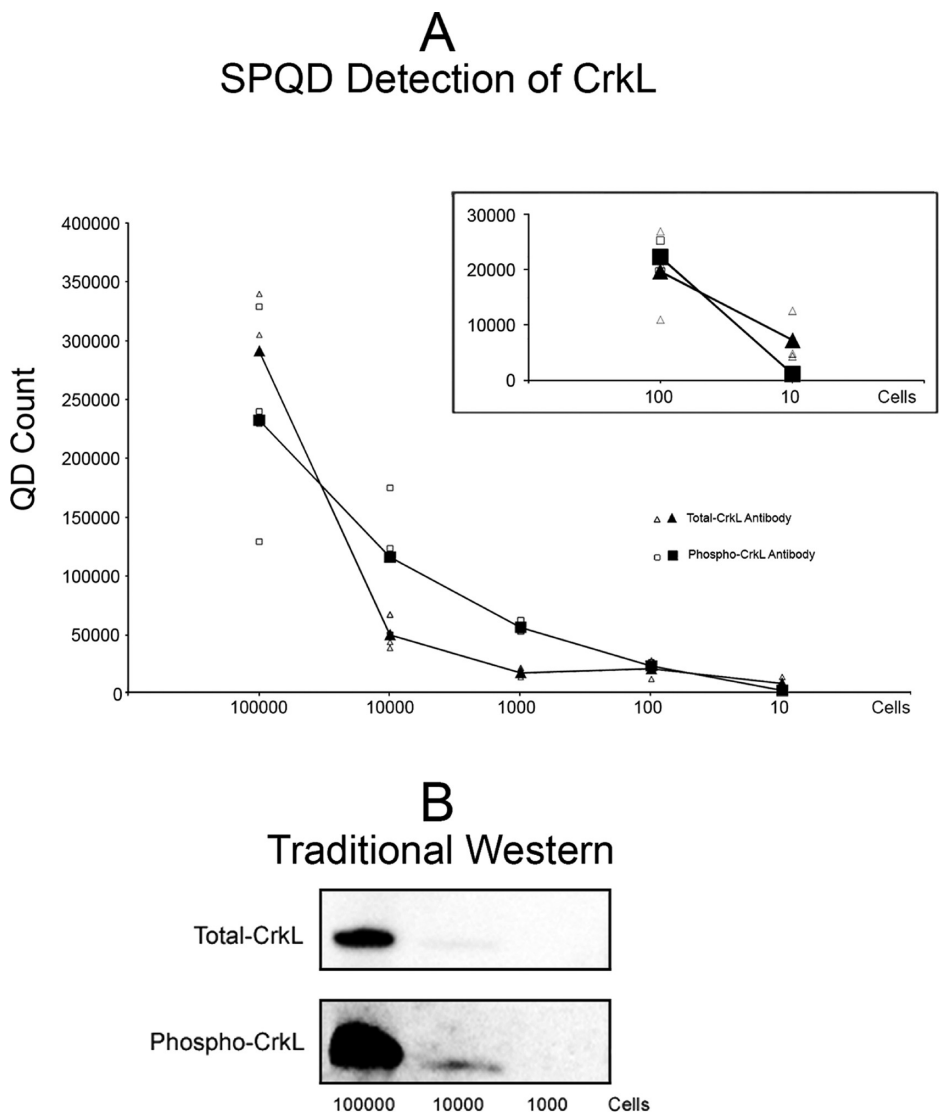

Figure 4. SPQD Western immunoblotting detects cellular CrkL protein in 100 cells. (A) Detection threshold for SPQD blots using total-CrkL and phosphorylated-CrkL antibodies in BCR-ABL positive CML cells, both show a detection threshold for 100 cells. Plot inset shows QD counts for the lowest cellular amounts (100 and 10 cells). SPQD Western QD counts for both CrkL antibodies were acquired from three independent experiments in a band area of 4 mm × 1 mm: (unfilled symbols) independent trials; (solid symbols) mean. (B) In comparison, traditional Western blots using the total-CrkL and phosphorylated-CrkL antibodies show a detection threshold of 100 000 and 10 000 cells, respectively. Blots were performed using the same cellular lysates, and gels were run simultaneously in each experiment.

ure 4B, top) and 10^2 times greater than traditional Westerns preformed with the phospho-CrkL antibody (Figure 4B, bottom). While the detectable threshold of SPQD Western blots will vary with the specific antibody and cell sample (*e.g.*, antibody affinity, amount of protein), similar results obtained for the detection of total-CrkL, phospho-CrkL, and TrkA proteins indicate that a threshold value of 100 cells can be regularly obtained.

Are the SPQD counts that are made on Western immunoblots composed of single QD or multiple QD tags? Single QDs can be detected on PDMS−PVDF transparent membranes (Supporting Information Movie 2S and Figure 3S), but during Western immunoblotting, other factors influence QD composition at each detected point of fluorescence. For example, more than one QD-streptavidin may bind to multiple biotin molecules on a single targeting antibody. Also, multiple targeting antibodies may bind to a single target protein macromolecule (depending on the number of antibody−protein recognition sites). In contrast, QD size and steric hindrance may limit the number of QD tags bound to each antibody−protein complex.

To determine the QD composition of single point counts, we analyzed the distribution of intensity values for each QD count and used the strict criterion of QD on−off blinking to distinguish single QDs from multiple QDs.[8,12,13] Analysis of membranes processed using SPQD Western blotting, both for purified Factor XI protein and cellular phosphorylated CrkL protein, shows discrete counts of QD fluorescence (Figure 5A, left and right, respectively). Using automated detection, each

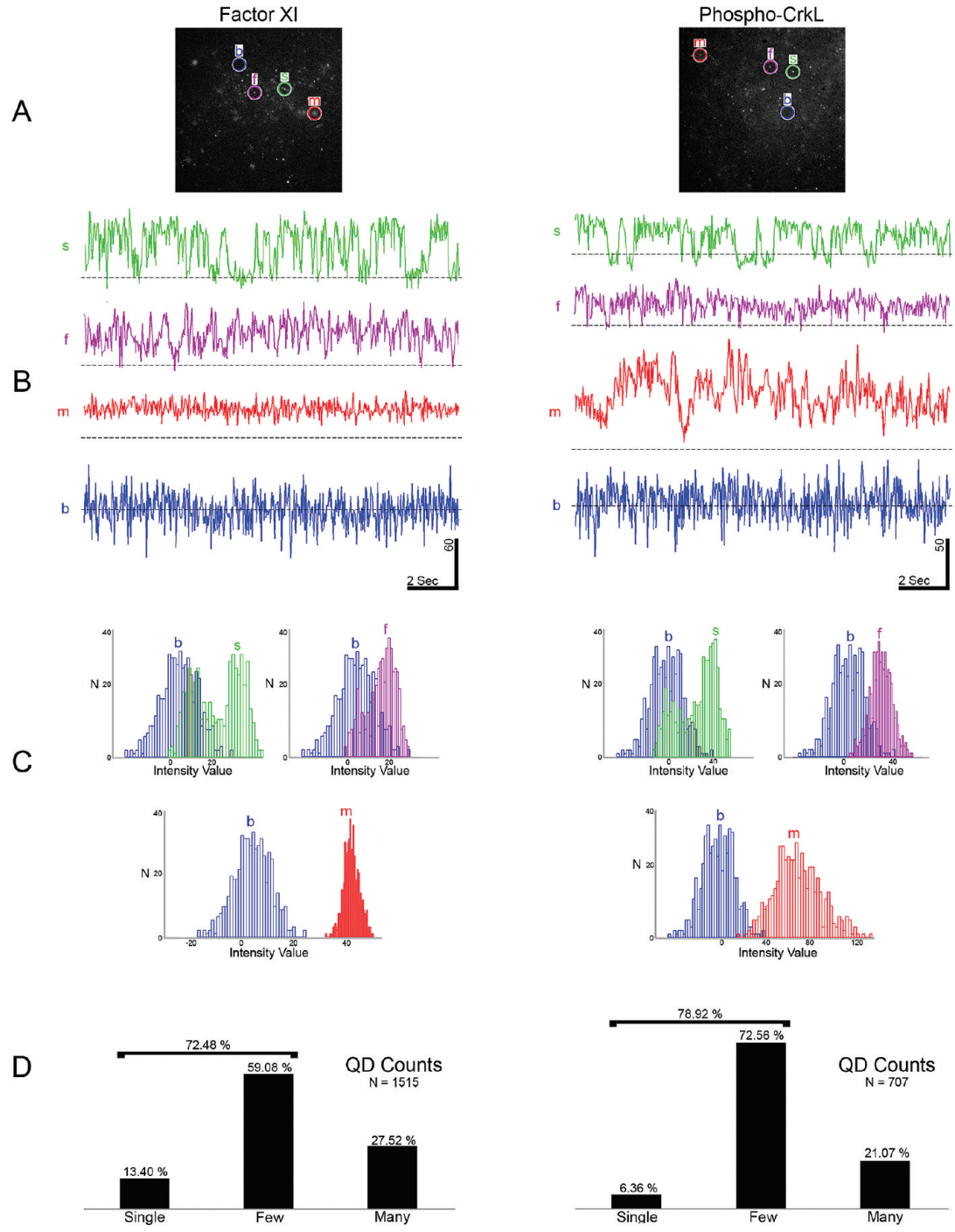

Figure 5. QD blinking analysis of Western blots of purified and cellular protein shows population of detected QD fluorescent counts composed of a single, few, and multiple QDs. (A) Single frame from movies of SPQD Western blots processed with purified Factor XI and cellular phospho-CrkL protein show examples of background fluorescence (b, blue), a single QD (s, green), a few QDs (f, purple), and many QDs (m, red). (B) Time-varying intensity traces corresponding to each circled location shown in A. Dashed lines in each trace indicate the mean background intensity value for each frame. Fluorescence counts associated with single QDs exhibit square wave on−off blinking behavior, counts associated with few QDs exhibit intensities that return to the mean background, and counts associated with many QDs exhibit a wide range of variance and intensity values that do not return to the mean background intensity. (C) Histograms plot the distribution of intensities for the profiles shown in B. QD counts composed of a single QD exhibit bimodal on−off blinking (s, green) which overlapped with the background distribution of intensities (b, blue). QD counts composed of a few QDs do not show a bimodal distribution (f, purple) but have a distribution of intensity values that overlap with the background intensity (b, blue). QD counts composed of many QDs show a distribution of values located above the mean background intensity (m, red). These distributions also exhibited a wide range of variances (compare red histograms for Factor XI and phospho-CrkL). (D) Bar graphs show the population of QD counts containing single, few, and many QDs. Single QDs make up 13.40 and 6.36% of the total QD counts for Factor XI blots (n = 1515, lanes loaded with 2 and 0.2 ng) and phospho-CkrL blots (n = 707, lanes loaded with 10 000 cells), respectively. The majority of all QD counts were composed single or a few (<9 QDs, see text): 72.48 and 78.92% for purified Factor XI and cellular phospho-CrkL, respectively.

SPQD count was located and its time-varying intensity profile was plotted. We found that SPQD counts exhibited three types of intensity profiles, distinguishable from areas on the membrane that did not contain QDs (Figure 5B, blue background traces). (1) Intensity profiles containing square wave on−off blinking indicated a QD point composed of a single QD (Figure 5B, green trace). (2) Intensity profiles that did not exhibit clear square wave on−off blinking but did exhibit intermittent intensity values that returned to a mean background intensity "off" state (Figure 5B, dashed line) indicated a QD count that blinked but was composed of a few QDs (Figure 5B, purple trace). (3) Remaining profiles contained low-frequency fluctuations that exhibited a wide range of variance but shared the common characteristic that their intensity profile did not return to the mean background intensity "off" state (*e.g.*, compare Figure 5B, red traces), indicating that the QD point consisted of many QDs and did not blink (Figure 5B, red trace). Histograms of intensity values reflected the distribution of intensities measured for each profile type (Figure 5C). Single blinking QDs showed a bimodal distribution of intensity values overlapping background intensity values when in the "off" state. QD counts composed of a few QDs showed a distribution of intensities values that were not bimodal-shaped but which overlapped with the histogram of background intensity values. QD counts containing many QDs showed a distribution of intensity values that were located above the mean background intensity. The distinguishing features from these histograms were used to categorize all QD counts into the categories of single, few, and many QDs. The results of this analysis, performed on purified Factor XI ($n = 1515$) and on cellular CrkL protein ($n = 707$), showed that single QDs made up 13.4 and 6.36% of the population of total QD counts. The majority of all QD counts were composed of either a single QD or a few QDs: 72.48 and 78.92%, respectively, for Factor XI and phospho-CrkL (see bar graph, Figure 5D).

How many QDs comprise "a few" QDs? We can estimate the maximum number of QDs in each detected blinking point by assuming that each single QD possesses a 50% on−off duty cycle. This means that, on average, n QDs are simultaneously in the off state for $1/(2^n)$ of the total time. For $n = 9$, all nine QDs would simultaneously be in the off state for 1/512, or 0.2%, of the time. Although this method of blinking analysis is preliminary, it provides an estimate that suggests that a majority of SPQD counts for both Factor XI and cellular phospho-CrkL were composed of nine QDs or less. In summary, QD fluorescent blinking analysis shows that, for SPQD Western blotting of both purified and cellular proteins, detection of single QD-tagged protein is possible and that a majority of detected fluorescence points are associated with single or a few (<9) QDs.

SUMMARY AND CONCLUSIONS

In this work, we showed that by using transparent PDMS−PVDF membranes, we can detect single points of QD fluorescence that were composed of a single or a few QDs, thereby achieving a new sensitivity limit for Western blotting. SPQD Westerns achieved an optimal sensitivity limit of 0.2 pg of pure protein and as few as 100 cells for cellular protein. This is a 10^3-fold improvement in detection sensitivity compared to traditional Westerns processed in parallel using the same membrane blots and a 10^2-fold reduction in the amount of required cell sample compared to bulk QD fluorescence-based Westerns (10 μg of cell protein as reported by Bakalova *et al.*).[5] Detection sensitivity for bulk QD-fluorescence-based Westerns could be increased with the attachment of multiple QDs to each antibody; however, this method provided a modest 2−5-fold increase in detection sensitivity.[5] By counting single fluorescent points, SPQD Westerns significantly extend the lower limit of detection for Western immunoblotting. This new sensitivity limit could make a difference in a number of applications where Western blotting would be the method of choice but cannot currently be employed due to insufficient detection sensitivity or sample availability.

What is the ultimate protein detection threshold for SPQD Western blotting? Given that the detection sensitivity of PVDF membrane-bound proteins is that of single QD fluorescent tags, other limiting factors are (1) the efficiency of protein transfer in the electroblotting process, (2) the affinity of the antibody probe used to detect PVDF membrane-bound proteins, and (3) the accuracy of QD−antibody probe binding and detection. While the efficiency of protein transfer during the electroblotting process will vary depending on the size and charge of the protein, electrotransfer can be extremely efficient under optimized conditions. Notably, the anti-NGF antibody we used in our studies did not possess remarkably high affinity (a high concentration of 1:500 streptavidin-HRP was needed to achieve optimized detection in our traditional Western immunoblots, Figure 2); yet, we were still able to attain sensitive detection with SPQD blotting. It might be possible to attain greater levels of sensitivity using even higher-affinity antibodies.

With regard to further increasing the detection sensitivity of SPQD Western blotting, an area of valuable future investigation is the optimization of QD counting to distinguish protein-tagged QDs (signal) from nonspecifically bound QDs (noise). A simple approach is to increase the number of sampled regions in a blot band in order to characterize with high resolution the spatial profile by which proteins gel-fractionate at low sample concentrations (*e.g.*, Gaussian-shaped band *vs* a rectangular-shaped blot band). Such a spatial profile may be then used as a template in all lanes to limit the locations in which QD counts are made. Mapping high-

resolution spatial profiles of QD-tagged proteins is feasible as automated scanning and QD counting are very rapid (30 min for automated blot scanning, 1 min per 200 images for automated counting). One challenge to note is that small changes in *z*-focus (at distances of approximately every 2 mm) need to be reliably corrected to retain and improve accuracy at these lower limits of sensitivity. Toward future work, we suspect that further optimization of SPQD Western immunoblotting along these lines could extend detection sensitivities into the range of subfemtogram quantities of protein and reduce samples to less than 100 cells.

METHODS

QD In-Gel Electrophoresis and Electroblotting. QDs were fractionated with high-resolution acrylamide-agarose (2% PA/0.5% AGE) electrophoresis and electroblotted to PVDF membranes as previously described.[6] Electrophoresis was performed at 100−150 V for 0.5−1.0 h in 1× TBE running buffer. QD samples were electroblotted to PVDF membranes in 0.5× TBE with 20% methanol under 100 V for 1−2 h.

SPQD Western Immunoblotting. Membranes containing fractionated QD bioconjugates (Figure 1) or incubated with antibody−QD bioconjugates (Figures 2−4) were air-dried on glass slides (>2 h). To render membranes transparent, QD-bound PVDF membranes were coated with polydimethylsiloxane (PDMS). We used Sylgard 184 silicone elastomer curing agent, a commercially available reagent (184 SIL ELAST Kit 3.9 kg, Ellsworth Adhesives), to make dry PVDF membranes transparent. Sylgard 184 silicone curing agent contains a variety of polydimethylsiloxanes including dimethyl, methylhydrogen siloxane; dimethylsiloxane dimethylvinyl-terminated; and tetramethyl tetravinyl cyclotetrasiloxane. Other polydimethylsiloxanes such as methyl-terminated polydimethylsiloxane, or the combination of siloxanes present in the base portion of Sylgard 184 elastomer, were also effective in converting PVDF for imaging single QDs. To make PVDF membranes transparent, air-dried PVDF membranes were immersed in 1 mL of PDMS in a glass dish for 10 s and then plated onto glass slides. Dry PVDF membranes became transparent instantly upon contact with the curing agent; it was critical that membranes were completely dry. Once membranes were transparent and coated with PDMS, they could be immediately imaged or stored at 4 °C for future use. Macroscopic QD-bound transparent PDMS−PVDF blots were viewed using a UV imaging system (UVP, MultiDoc-It). Microscopic images of PDMS−PVDF membranes were acquired using a fluorescent microscope (Zeiss Axiovert 200M) equipped with 40 and 100X objectives, excitation and emission filters (Chroma), and a cooled monochrome CCD camera (Axiocam). Automated microscope field images were taken using a precise *x*−*y* scanning stage (ASI) under software control (AxioVision). The membrane is a 3D object containing proteins, which may penetrate the blot during electrotransfer, and QDs, which may diffuse into the blot during incubation of the membrane with antibody−QD probes. While sectioning the entire 3D membrane blot is possible, this effort provides little gain since the period of membrane electrotransfer can be reduced to deposit the majority of proteins onto the membrane surface. We made relative comparisons of protein amount across different lanes by analyzing QD-tagged proteins residing at the surface plane of the membrane blot, the location where the majority of QDs were found. To obtain profiles of gel lanes, single counts of QDs were taken along the length of a gel lane starting at the center of the loading well. The position of the bands was located using molecular weight markers (161−0374, Bio-Rad; P7708s, NEB; LC6925, Invitrogen) either in adjacent or in the same lane, as well as by correspondence of macroscopic fluorescence with adjacent well lanes. The same imaging parameters of integration time and band position were applied to all bands in a membrane blot.

Automated QD Counting. QD counts were made from fluorescence images using a custom-written procedure that is based on the algorithm developed by Crocker and Grier and implemented with the help of publicly available Matlab scripts.[19,20] CCD-collected fluorescence microscopy images are first conditioned using a spatial band-pass filter characterized by two cutoff feature sizes. The small feature cutoff of the band-pass filter is tuned to reduce pixel noise, while the large feature cutoff is adjusted to eliminate inhomogeneous illumination and background fluorescence. A threshold is then applied to the filtered image, leaving only a small region of high intensity corresponding to each particle; the pixel with maximum intensity out of each region is chosen as the preliminary location for that particle. Subsequent processing refines the preliminary locations by finding the centroid of the intensity pattern near the preliminary location. This particle location procedure is carried out on multiple sampled images in each membrane lane, giving refined particle locations that are counted and form an estimate for the number of QD counts per lane for each experiment. This automated QD count algorithm produces 90% accuracy of automated QD counts, as compared to QD counts obtained by human eye on the same images. QD blinking produces negligible error in these automated counts. By noting the locations of all individual QD counts and making accumulated counts over multiple frames in a movie, QDs in an "off" state for one image frame will eventually return to their "on" state in another image frame and can be counted. When we compare counts made from one frame *versus* counts made over multiple frames of an entire movie, we find that QD counts made from single image frames produce an error of 15% of total QD counts under our imaging capture rates. Given that a typical image frame consists of a total of 200 QDs, we will miss only 30 QDs/image frame.

QD Blinking Analysis. Movies of SPQD Western blots were acquired with an Andor iXon camera at 33 frames per second for 500 frames. A total of six movies were collected from CrkL SPQD Westerns and nine movies from Factor XI SPQD Westerns. The detection algorithm designed for automated QD counting (see above) was used in each frame to detect the locations of discrete QD counts, and an algorithm was created to output all QD count locations for a given number of frames. Pixel intensity values were measured at each QD count location in each frame. To measure background noise in each frame, we acquired background pixel intensity values which were not at QD count locations. Because the background noise varies for each movie, we normalized our measurements using a background subtraction. In each movie, we calculated the mean background pixel intensity and subtracted this value from all QD count measurements and background measurements across frames. For each movie, a baseline threshold was used to distinguish between QD count profiles exhibiting blinking behavior and those which never demonstrated an "off" state. We then characterized each QD count profile as consisting of either single, few, or many QDs. QD count profiles exhibiting intermittent intensity values that returned to the baseline threshold showed square wave on−off blinking behavior and had a bimodal distribution of intensity values that were categorized as single QDs. QD count profiles exhibiting intermittent intensity values that returned to the baseline threshold, but did not have a bimodal distribution of intensity values, were categorized as a few QDs ($n < 9$); see Results. QD count profiles having pixel intensity values only above the baseline threshold were categorized as groups of many QDs.

Detection of Purified Factor XI and NGF Protein Standards. Serial dilutions of NGF (#1156-NG/CF, R&D Systems) and Factor XI were fractionated using 12 and 8% SDS−PAGE, respectively. Each lane containing protein target was flanked by lanes containing molecular weight markers. Samples were electroblotted onto to PVDF membranes, and membranes were blocked with 5% BSA in TBS/0.1% Tween20 overnight. Biotinylated anti-NGF (0.1 mg/mL, R&D Systems) and biotinylated anti-Factor XI (6.6 mg/mL, a generous gift from Dr. Andras Gruber, Oregon Health and Sci-

ence University) were prepared using previously described biotinylation methods.[21] Briefly, a mixture containing 20 times the number of moles of biotin as moles of antibody is set on ice overnight and then dialyzed for 3 h at room temperature; this is expected to produce 3−5 biotins per antibody (Pierce, technical specifications).

SPQD Blotting of NGF and Factor XI: Anti-NGF-biotin-strep-QD655 probes were made with a molar ratio of anti-NGF to strep-QD655 of 4:1 (0.2 μg/mL anti-NGF and 0.3 nM streptavidin-QD655), and blots were incubated with this probe for 1 h at room temperature. Factor-XI-fractionated membranes were first incubated with 6 μL of 6.4 mg/mL biotinylated Factor XI 1A6 antibody overnight at 4 °C and then followed by incubation with 40 μL of 15 nM streptavidin-QD655 at room temperature. Blots were analyzed by single QD counting (see above).

Traditional Western Immunoblotting NGF: NGF-fractionated membranes were incubated with 2 μg/mL biotinylated anti-NGF for 1 h. After extensively washing, blots were incubated with streptavidin-HRP (1:1000, #21126, Pierce) for 1 h. After washing, membranes were immersed into SuperSignal West Pico Chemiluminescent substrate (#34077, Pierce) for 5 min and exposed to X-ray film for 3 min. All Western immunoblot assays were optimized to achieve the best detectable signal.

Traditional Western Immunoblotting Factor XI: Purified Factor XI was loaded into the stacking gel without β-mercaptoethanol. Gels were run at 100 V until samples reached the resolving gel and then run at 125 V until the first ladder marker reached the bottom (7 kD, P7708s, NEB). Electroblotted samples were blocked, incubated overnight with 6 μL of 6.4 mg/mL biotinylated Factor XI 1A6 antibody at 4 °C, washed, blocked again, and then incubated with streptavidin-HRP (1:5000) for 1.5 h at room temperature. Blots were then washed and exposed to X-ray film for 2−10 s.

Detection of TrkA Receptor Protein from Cellular Lysates. PC12 cells were stimulated with NGF (100 ng/mL, R&D Systems, #1156-NG/CF) for 1 h. Whole cell extracts were prepared with lysis buffer (50 mM Tris-HCl, pH7.4, 150 mM NaCl, 1%NP-40, 0.1% sodium deoxycholate, 4 mM EDTA) supplemented with protease inhibitor cocktail (#P2714-1BTL Sigma). Insoluble materials were removed from the protein extract by centrifugation at 13 000 rpm for 15 min. Serial diluted cell lysates were mixed with 1× laemmli sample buffer (#161-0737, Bio-Rad) and denatured (95 °C, 5 min). Lysates were separated with 8% SDS−PAGE. Samples were loaded into gels with flanking lanes containing molecular weight markers. Extracts from control (no NGF stimulation) cells were run in parallel as a control. After electroblotting onto to PVDF membranes, membranes were blocked with 5% BSA in TBST overnight.

SPQD Blotting of TrkA: Blots were incubated with anti-TrkA-biotin-strep-QD655s (4 anti-TrkA Ab:1 strep-QD655 molar ratio, 0.2 μg/mL anti-TrkA and 0.3 nM strep-QD655) for 1 h, or anti-β-actin-biotin-strep-QD655s (1 anti-β-actin Ab:1 strep-QD655, molar ratio, 0.0045 μg/mL anti-β-actin, 0.03 nM strep-QD655) for 1 h. Blots were analyzed by single QD counting (see above).

Traditional Western Immunoblotting of TrkA: Blots were incubated with biotinylated anti-TrkA antibody (4 μg/mL, sc-11, C-14, Santa Cruz) for 1 h, or with control biotinylated β-actin antibody (0.01 μg/mL, #4967, Cell Signaling) for 1 h. After extensive washing, blots were incubated with streptavidin-HRP (1:5000) for 1 h. Membranes were immersed into SuperSignal West Pico chemiluminescent substrate for 5 min, then exposed to X-ray film for 3 min.

Detection of CrkL and Phosphorylated-CrkL Protein from Cellular Lysates. Serially diluted imatinib-treated Mo7e/p210 cellular lysate (starting concentration: 10^5 per 20 μL) was loaded into four identical precast 4−15% Criterion Tris-glycine gels. Each gel was run at 200 V for 1 h, until the first ladder band reached the gel bottom (4 kD, LC6925, Invitrogen). Samples were electroblotted to PVDF membranes at 95 V for 1 h and then blocked overnight in 3% BSA in TBST overnight at 4 °C.

SPQD Blotting of CrkL and Phospho-CrkL: One membrane was incubated with 10 mL of biotinylated anti-CrkL (1:2500 in 3% BSA/TBST), and another membrane was incubated with 10 mL of biontinylated antiphospho-CrkL (1:2500 in 3% BSA/TBST), both at 4 °C for 2 h. Both membranes were washed and then incubated with 200 μL of 1 nM strep-QD655 for 1 h at room temperature. Blots were analyzed by single QD counting (see above).

Traditional Western Immunoblotting of CrkL and Phospho-CrkL: One membrane was incubated with 25 mL of anti-CrkL (1:2500 in 3% BSA/TBST), and another membrane was incubated with 25 mL of biontinylated antiphospho-CrkL (1:2500 in 3% BSA/TBST), both at 4 °C overnight. For both membranes, 15 s exposures were obtained using a Lumi Imager (Roche).

Acknowledgment. We thank Jiaqing Pang and Lauren T. Adrian for their excellent technical assistance with Western blotting, Joseph Chung for writing an early version of the QD counting program, Dr. Andras Gruber for the generous gift of anti-Factor XI antibody, and Dr. Sean Gallagher for the generous gift of a UVP gel transilluminator. We gratefully acknowledge the support of DOD (W81XWH-07-2-0107) and Oregon ETIC funds (T.Q.V.).

Supporting Information Available: Additional figures and movie. This material is available free of charge *via* the Internet at http://pubs.acs.org.

REFERENCES AND NOTES

1. Burnette, W. N. "Western Blotting": Electrophoretic Transfer of Proteins from Sodium Dodecyl Sulfate−Polyacrylamide Gels to Unmodified Nitrocellulose and Radiographic Detection with Antibody and Radioiodinated Protein A. *Anal. Biochem.* **1981**, *112*, 195–203.
2. Magi, B.; Liberatori, S. Immunoblotting Techniques. *Methods Mol. Biol.* **2005**, *295*, 227–254.
3. Johnson, C. J.; Zhukovsky, N.; Cass, A. E.; Nagy, J. M. Proteomics, Nanotechnology and Molecular Diagnostics. *Proteomics* **2008**, *8*, 715–730.
4. Ornberg, R. L.; Harper, T. F.; Liu, H. Western Blot Analysis with Quantum Dot Fluorescence Technology: A Sensitive and Quantitative Method for Multiplexed Proteomics. *Nat. Methods* **2005**, *2*, 79–81.
5. Bakalova, R.; Zhelev, Z.; Ohba, H.; Baba, Y. Quantum Dot-Based Western Blot Technology for Ultrasensitive Detection of Tracer Proteins. *J. Am. Chem. Soc.* **2005**, *127*, 9328–9329.
6. Liu, H. Y.; Vu, T. Q. Identification of Quantum Dot Bioconjugates and Cellular Protein Co-Localization by Hybrid Gel Blotting. *Nano Lett.* **2007**, *7*, 1044–1049.
7. Chan, W. C.; Nie, S. Quantum Dot Bioconjugates for Ultrasensitive Nonisotopic Detection. *Science* **1998**, *281*, 2016–2018.
8. Michalet, X. Quantum Dots for Live Cells, *In Vivo* Imaging, and Diagnostics. *Science* **2005**, *307*, 538–544.
9. Pattani, V. P.; Li, C.; Desai, T. A.; Vu, T. Q. Microcontact Printing of Quantum Dot Bioconjugate Arrays for Localized Capture and Detection of Biomolecules. *Biomed. Microdevices* **2008**, *10*, 367–374.
10. Sperling, L. H.; Mishra, V. The Current Status of Interpenetrating Polymer Networks. *Polym. Adv. Technol.* **1995**, *7*, 197–208.
11. Lucas, P.; Robin, J. J. Silicone-Based Polymer Blends: An Overview of the Materials and Processes. *Adv. Polym. Sci.* **2007**, *209*, 111–147.
12. Michalet, X.; Pinaud, P.; Lacoste, T. D.; Dahan, M.; Bruchez, M. P.; Alivisatos, A. P.; Weiss, S. Properties of Fluorescent Semiconductor Nanocrystals and Their Application to Biological Labeling. *Single Mol.* **2001**, *2*, 261–276.
13. Nirmal, M.; Dabbousi, B. O.; Bawendi, M. G.; Macklin, J. J.; Trautman, J. K.; Harris, T. D.; Brus, L. E. Fluorescence Intermittency in Single Cadmium Selenide Nanocrystals. *Nature* **1996**, *383*, 802–804.
14. Schmidt, H. D.; Duman, R. S. The Role of Neurotrophic Factors in Adult Hippocampal Neurogenesis, Antidepressant Treatments and Animal Models of Depressive-Like Behavior. *Behav. Pharmacol.* **2007**, *18*, 391–418.

15. Allen, S. J.; Dawbarn, D. Clinical Relevance of the Neurotrophins and Their Receptors. *Clin. Sci.* **2006**, *110*, 175–191.
16. Tucker, E. I.; Marzec, U. M.; White, T. C.; Hurst, S.; Rugonyi, S.; McCarty, O. J.; Gailani, D.; Gruber, A.; Hanson, S. R. Prevention of Vascular Graft Occlusion and Thrombus-Associated Thrombin Generation by Inhibition of Factor XI. *Blood* **2009**, *113*, 936–944.
17. Druker, B. J. Efficacy and Safety of a Specific Inhibitor of the Bcr-Abl Tyrosine Kinase in Chronic Myeloid Leukemia. *N. Engl. J. Med.* **2001**, *344*, 1031–1037.
18. Talpaz, M. Dasatinib in Imatinib-Resistant Philadelphia Chromosome-Positive Leukemias. *N. Engl. J. Med.* **2006**, *354*, 2531–2541.
19. Crocker, J. C.; Grier, D. G. Methods of Digital Video Microscopy for Colloidal Studies. *J. Colloid Interface Sci.* **1996**, 179.
20. http://physics.georgetown.edu/matlab/.
21. Vu, T. Q.; Maddipati, R.; Blute, T. A.; Nehilla, B. J.; Nusblat, L; Desai, T. A. Peptide-Conjugated Quantum Dots Activate Neuronal Receptors and Initiate Downstream Signaling of Neurite Growth. *Nano Lett.* **2005**, *5*, 603–607.